NUMERICAL SIMULATION OF GAS-LIQUID TWO-PHASE CONVECTIVE HEAT TRANSFER IN A MICRO TUBE

Poychat Ua-arayaporn*, Koji Fukagata*, Nobuhide Kasagi*, and Takehiro Himeno°

*Department of Mechanical Engineering, The University of Tokyo
Hongo 7-3-1, Bunkyo-ku, Tokyo, 113-8656, Japan
°Department of Aeronautics and Astronautics, The University of Tokyo
Hongo 7-3-1, Bunkyo-ku, Tokyo, 113-8656, Japan

ABSTRACT

Numerical simulation of an air and water two-phase flow in a micro tube is carried out. A special focus is laid upon the flow and heat transfer characteristics in slug flows. An axisymmetric two-dimensional flow is assumed. The governing equations are the same as those ordinarily used for flows in macro-sized tube, and are solved by using the finite difference method. The interface of gas and liquid is captured by the level set method. In each simulation, the mean pressure gradient and the wall heat flux are kept constant. The simulation is repeated under different conditions of pressure gradient and void fraction. The superficial Reynolds numbers of the gas and liquid phases studied are 0.2-10 and 14-435, whilst the superficial Weber numbers of gas and liquid phases are 0.0017-0.03 and 0.4-130, respectively. Regardless of the flow parameters, the gas-phase velocities are found approximately 1.2 times higher than the liquid-phase velocity. This is in accordance with the Armand correlation valid for two-phase flows in macro-sized tubes, but not with the experimental data of micro tubes. The computed wall temperature distribution is qualitatively similar to that observed experimentally in a mini channel. The local Nusselt number beneath the bubble is found notably higher than that of single-phase flow.

INTRODUCTION

Flow in a micro conduit has become very important in many emerging applications such as micro heat exchangers and Lab-on-a-chip. In order to successfully design such devices, understanding of flow physics in micro scale and their engineering modeling are crucial.

Gas-liquid two-phase flows in mini and micro conduits often exhibit different behavior as compared to those in macro-sized conduits. One reason for this difference is the ratio of the gravitational effects to the surface tension, which can be represented by the Eötvös number (or the Bond number),

$$Eo = \frac{g\Delta\rho d^2}{\sigma}, \qquad (1)$$

where g, $\Delta\rho$, d and σ denote the gravitational acceleration, the density difference between two phases, the hydraulic diameter of conduit, and the surface tension. For instance, Brauner et al. [1] propose a criterion, $Eo << (2\pi)^2$, for the surface tension to be dominant.

As reviewed, e.g., by Kandlikar [2], extensive experimental studies have been reported on gas-liquid two-phase flow and boiling heat transfer in mini and micro conduits. The primary concerns are the pressure drop and heat transfer characteristics under given flow conditions. However, there seem to still exist considerable discrepancies between experimental data, especially in heat transfer characteristics, largely due to the extreme difficulty in experimental setup and measurement.

Our final goal is to perform systematic simulation of boiling heat transfer in micro conduit in order to obtain comprehensive understanding of two-phase flow physics and heat transport mechanisms in micro conduits. As the first step, we investigate the essential mechanisms of isothermal two-phase slug flow and convective heat transfer without phase change. The global properties obtained in the simulation are compared with available experimental data and empirical correlations. The underlying mechanisms are discussed based on the computed flow characteristics.

SIMULATION METHODS

Governing equations

We consider a gas-liquid two-phase flow in a cylindrical pipe. Each phase is treated as incompressible. The gas and liquid are immiscible and phase change does not take place. Under these conditions, the fluid velocity field, $\vec{u}$, is given by the continuity equation,

$$\nabla \cdot \vec{u} = 0, \qquad (2)$$

and the momentum equation,

$$\frac{\partial(\rho\vec{u})}{\partial t} + \vec{u}\cdot\nabla(\rho\vec{u}) = -\nabla p + \nabla\cdot(2\mu D) - \sigma\kappa\delta\vec{n}, \qquad (3)$$

where ρ, μ, and D denote the density, the dynamic viscosity, and the stress tensor, respectively. The last term of Eq. (3) represents the surface tension force, with κ, δ, and $\vec{n}$ denoting the curvature, the Dirac delta function, and the unit normal vector of the interface, respectively. The gravitational force

term is omitted because Eo is estimated on the order of 10^{-4} under the conditions assumed in the present study.

We also consider heat transfer. By assuming small temperature difference, the temperature is treated as a passive scalar. Thus, the governing equation for temperature, T, reads

$$\frac{\partial(\rho C_p T)}{\partial t} + \vec{u}\cdot\nabla(\rho C_p T) = \nabla\cdot(\lambda\nabla T), \tag{4}$$

where C_p and λ are the specific heat at constant pressure and the heat conductivity, respectively.

Note that Eqs. (2)-(4) are satisfied in both gas and liquid phases.

Interface tracking method

In order to accurately capture the gas-liquid interface, we adopt the level set method [3]. The interface is captured implicitly as the zero level set of a smooth function, which is denoted as F; the gas-liquid interface is identified as $F = 0$. The level set function is negative in the gas ($F < 0$) and positive in the liquid ($F > 0$). The function of F is given by the following advection equation:

$$\frac{\partial F}{\partial t} + \vec{u}\cdot\nabla F = 0. \tag{5}$$

The physical properties of the fluid are calculated by interpolating those of the gas and liquid phases, according to

$$\phi = 0.5(\phi_L + \phi_G) + H_\varepsilon(\phi_L - \phi_G). \tag{6}$$

Here, ϕ denotes any physical property (ρ, μ, C_p, and λ) and its subscripts, L and G, denote the liquid and gas, respectively. The interpolation function H_ε is a smoothed Heaviside function defined as:

$$H_\varepsilon(F) = \begin{cases} -0.5 & \text{for } F \le -\varepsilon \\ 0.5\left[\left(\frac{F}{\varepsilon}\right) + \frac{1}{\pi}\sin\left(\frac{\pi F}{\varepsilon}\right)\right] & -\varepsilon < F < \varepsilon \\ 0.5 & F \ge \varepsilon, \end{cases} \tag{7}$$

where ε is the width of interface smoothing. In the present simulation, ε is equal to the length of thress computational grids.

The surface tension term in Eq. (3) is computed by using the continuum surface force model [4]. The Dirac delta function in the surface tension term is replaced by a smoothed Dirac delta function, δ_ε, which is defined as

$$\delta_\varepsilon(F) = \frac{dH_\varepsilon}{dF} = \begin{cases} 0.5\left[\frac{1}{\varepsilon} + \frac{1}{\varepsilon}\cos\left(\frac{\pi F}{\varepsilon}\right)\right] & \text{for } |F| < \varepsilon \\ 0 & \text{otherwise.} \end{cases} \tag{8}$$

The curvature of the interface is calculated by

$$\kappa = \nabla\cdot\vec{n}, \tag{9}$$

where the unit vector normal to the interface is computed from the level set function, i.e.,

$$\vec{n} = \nabla F / |\nabla F|. \tag{10}$$

Numerical procedure

The governing equations are solved by the SMAC method [5]. An equally spaced staggared mesh system is adopted. The second-order accurate central difference scheme is used for the spatial discretization. The pressure Poisson equation is solved by using the SOR scheme.

Integration of the level-set equation, Eq. (4), is done by the CIP scheme [6]. The level-set function F is designed as a distance function, which measures the distance from the bubble surface. However, this nature is not simply conserved by Eq. (4). Maintaining F as a distance function is essential for providing the correct interface force and the fixed interface thickness. Thus, the re-initialization procedure [3] is made at every computational time step. Moreover, in order to conserve the mass of bubble, a mass correction procedure is introduced when the error of mass exceeds the given criterion. The details of the CIP level-set method used here are found in [7].

The CIP scheme is also used here for the advection term of the energy equation of (4) in order to capture steep temperature gradients, which are expected near the gas-liquid interface.

Flow and boundary conditions

In the present study, only the bubble-train and slug flow regimes are considered. Thus, the flow is assumed axisymmetric, so a two-dimensional (r-z) computational domain is employed. The periodic boundary condition is applied at the both ends. The length of computational domain is set to $L = 4R$ in most of the cases. No-slip condition is applied at the wall.

For the temperature field, a uniform wall heat flux is assumed. A quasi-periodic boundary condition,

$$\left.\frac{\partial T}{\partial z}\right|_{z=0} = \left.\frac{\partial T}{\partial z}\right|_{z=L}, \tag{11}$$

is applied on the both ends. Note that this formulation is ill-posed, because all the boundary conditions are of the Neumann type. The temperature field computed with this formulation (denoted as T_{sim}) contains an unknown temperature, T_u, in addition to the actual temperature, T, i.e.,

$$T_{sim}(r,z,t) = T(r,z,t) + T_u(t). \tag{12}$$

In order to obtain the actual temperature, the value of T_u should be computed from the global energy balance. In the present study, however, this procedure is omitted because only the temperature difference is of interest.

ISOTHERMAL TWO-PHASE FLOW

We assume water and air at 25 °C, 1 atm and the radius R of the cylindrical tube is fixed at 10 μm. The condition is similar to that in the experiment by Serizawa et al. [8]. The simulation is performed for different values of void fraction, α, and pressure gradient, $-dP/dz$. Each simulation is started with gas and liquid at rest. One bubble is initially placed in the computational

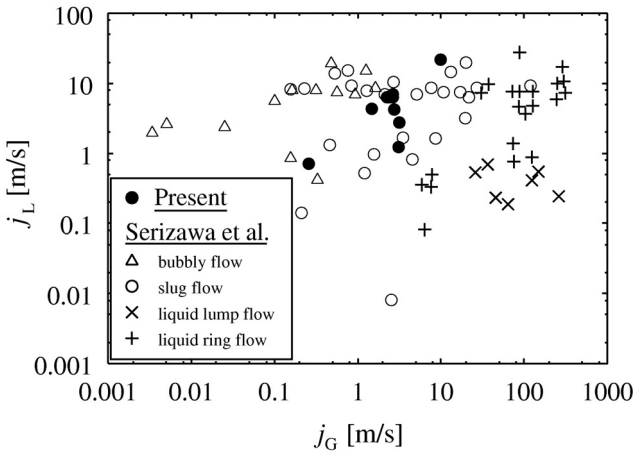

Fig. 1: Superficial velocities of air-water flow in 20 μm ID tube.

domain. The pressure gradient is kept constant and the simulation is continued until the flow becomes fully developed.

Global quantities

Figure 1 shows the computed superficial gas and liquid velocities, j_G and j_L, which are defined respectively as

$$j_G = \frac{Q_G}{A}, \qquad j_L = \frac{Q_L}{A}, \tag{13}$$

where Q_G and Q_L are the volumetric flow rates of the gas and liquid and A is the cross-sectional area of the pipe. Ten cases were simulated with $-dP/dz = 8.5\times10^{1}$–3.0×10^{3} MPa/m and α= 0.2–0.8. The resultant superficial Reynolds numbers of the gas and liquid phases studied are 0.2-10 and 14-435, respectively. The superficial Weber numbers of gas and liquid phases are 0.0017-0.03 and 0.4-130, respectively. In all cases, the computed superficial velocities are in the range of slug flow regime in the experiment of Serizawa et al. [8].

The frictional pressure loss is compared with the Lockhart-Martinelli model [9]. Namely, the two-phase pressure gradient, $(-dP/dz)_{TP}$, is evaluated through the two-phase multiplier, Φ, and the Lockhart-Martinelli parameter, X, defined respectively as

$$\Phi^2 = \frac{(-dP/dz)_{TP}}{(-dP/dz)_{LO}}, \tag{14}$$

and

$$X^2 = \frac{(-dP/dz)_{LO}}{(-dP/dz)_{GO}}. \tag{15}$$

Here $(-dP/dz)_{LO}$ and $(-dP/dz)_{GO}$ represent the pressure gradients when the liquid and gas separately flow at their superficial velocities.

The relation between Φ and X is usually given by the Chisholm correlation [10], which reads

$$\Phi^2 = 1 + \frac{C}{X} + \frac{1}{X^2}, \tag{16}$$

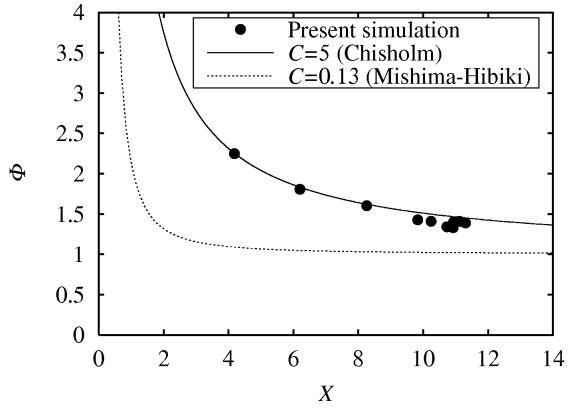

Fig. 2: Lockhart-Martinelli correlation.

where C is the Chisholm parameter, of which value ranges between 5 and 21; C =5 corresponds to a laminar flow and C = 21 to a turbulent flow. More recently, Mishima and Hibiki [11] suggested a modified expression by correlating their experimental data of air-water flow in mini-tubes of 1 to 4 mm in inner diameter. The Chisholm parameter in Mishima-Hibiki model is diameter-dependent and can be expressed as

$$C = 21\left[1 - \exp(-0.319\,d)\right], \tag{17}$$

where the inner diameter, d, is given in millimeter. In the present case of d = 0.02, Eq. (17) gives C = 0.13.

Figure 2 shows the relation between Φ and X in the present simulation. In contrast to the previous experimental studies with micro and mini tubes, the present data are in excellent agreement with the original Chisholm correlation with C = 5 rather than Mishima-Hibiki model (C = 0.13) proposed for micro and mini tubes.

Effects of pressure gradient

Effects of different pressure gradient are studied in some detail. The void fraction is fixed at α= 0.2. As depicted in Fig. 3a, the bubble is nearly spherical under a weak pressure gradient ($-dP/dz$ = 85 MPa/m). Also shown in the figure are the streamlines relative to the bubble velocity. An anti-clockwise circulation is found inside the bubble. The circulation is strong in the region close to the wall, where the gas-liquid interface is driven backward due to the strong shear. A circulation can also be found in the liquid region, and it results in continuous refreshment of the liquid layer near the wall and enhances the momentum transfer to the wall. Namely, the pressure drop increases due to this circulation. A similar circulation pattern has been shown experimentally [12] and theoretically [13]. With the increase in pressure gradient, the bubble becomes longer as shown in Figs. 3b and 3c. In these cases, circulation is found also around the head of the bubble. It is clockwise and corresponds to the elongation of bubble.

Figure 4 shows the mean gas phase velocity, U_G, the mean liquid velocity, U_L, and the mean two-phase velocity, U_{TP}, computed under different pressure gradients. These velocities are defined respectively as

$$U_G = \frac{Q_G}{\alpha A} = \frac{j_G}{\alpha}, \qquad U_L = \frac{Q_L}{(1-\alpha)A} = \frac{j_L}{1-\alpha}, \tag{18}$$

and

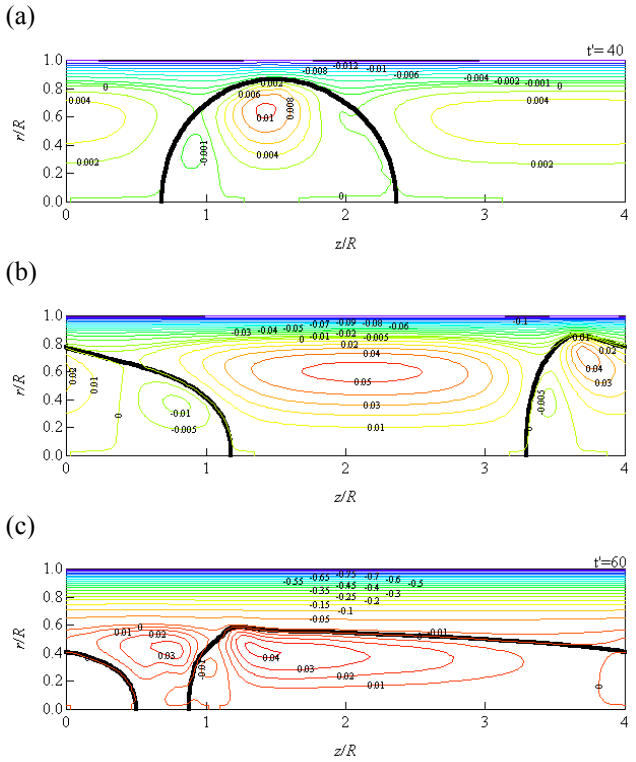

Fig. 3: Bubble shape and relative streamlines under different pressure at $\alpha = 0.2$ in $R = 10$ μm tube. (a) $-dP/dz = 85$ MPa/m; (b) 850 MPa/m; (c) 3200 MPa/m.

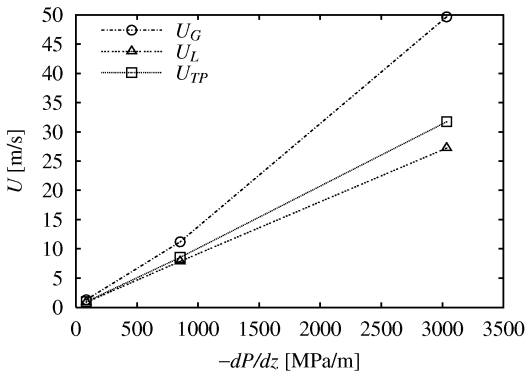

Fig. 4: Gas phase velocity (U_G) and two-phase velocity (U_{TP}) under different pressure gradient ($\alpha = 0.2$, $R = 10$ μm).

$$U_{TP} = \frac{Q_G + Q_L}{A} = j_G + j_L. \tag{19}$$

With the increase of pressure gradient, all of these velocities increase almost linearly. The ratio of U_G to U_{TP} is slightly higher for a larger pressure gradient. The reason for this is indicated by the change of bubble shapes as shown in Fig. 3. With the increase of pressure gradient, the bubble is elongated in the central region of pipe and less influenced by the no-slip wall. Thus, the velocity ratio is higher than that under a low pressure gradient.

Effects of void fraction

Figure 5 shows the computed relation between the void fraction α and the gas volumetric flow ratio β defined as

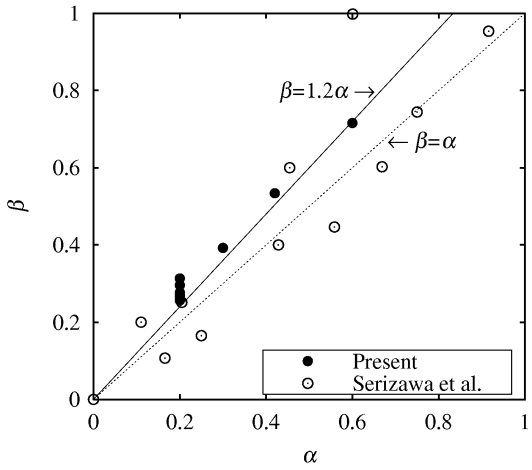

Fig. 5: Relation between void fraction, α, and volumetric flow ratio, β.

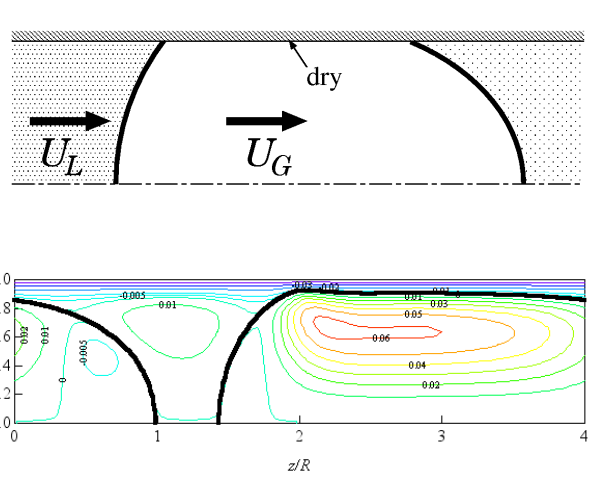

Fig. 6: Bubble shape in slug flow regime. (a) Probable shape in previous experiments (dry wall); (b) Present simulation with $\alpha = 0.6$, $-dP/dz = 430$ MPa/m (wet wall).

$$\beta = \frac{Q_G}{Q_G + Q_L} = \frac{j_G}{j_G + J_L} = \alpha \frac{U_G}{U_{TP}}. \tag{20}$$

Multiple plots for $\alpha = 0.2$ correspond to different pressure gradients and different sizes of computational box (discussed later). The relation between α and β is found nearly linear and well in accordance with the Armand correlation [14] proposed for conventional tubes, which reads

$$\beta = 1.2\alpha. \tag{21}$$

The results are also compared with bubbly and slug flows in experiment of Serizawa et al. [8]. The experimental data, however, seem to be distributed around the line of $\beta = \alpha$.

The discrepancy between the present simulation results and the experimental data can be explained as follows, at least for the case of high void fraction. As is noted by Serizawa et al. [8], a dry zone may have been developed under the gas slug in their experiment. Therefore, the gas, liquid and two-phase velocities become all equal, as schematically shown in Fig. 6a. Hence,

$\alpha/\beta = U_{TP}/U_G = 1$. In the present simulation, however, the wall is always wet as exemplified in Fig. 6b. The possible reason for this failure is the lack of special treatment for gas-liquid-solid interfaces. Due to the no-slip wall, the liquid film between the bubble and the wall has always a lower velocity than the gas velocity and this fact results in U_{TP} smaller than U_G (i.e., $\beta > \alpha$). Note that this argument also consistently explains the discrepancy in the two-phase multiplier shown in Fig. 2.

TWO-PHASE FLOW HEAT TRANSFER

In all cases, the physical properties of fluids are evaluated at $T = 373$ K.

Figure 7 shows the temperature contours at $\alpha = 0.2$ under different pressure gradients. Under the smaller pressure gradient (Fig. 7a), where the bubble shape is kept nearly spherical, the temperature contours inside the liquid slug align nearly parallel. Effects of convection due to the anticlockwise circulation shown in Fig. 3a are noticed around the front and rear ends of the bubble. The situation is basically similar under the larger pressure gradient (Fig. 7b), although the temperature in the central region is more homogenized due to the stronger circulation in the liquid slug. In both cases, the temperature in the bubble is closer to the wall temperature and more homogeneous due to the larger thermal diffusivity.

Figure 8 shows the streamwise distribution of the wall and bulk mean temperatures in the corresponding cases. Here, the temperatures are made dimensionless by using the domain-averaged wall and bulk mean temperatures, $<T_w>$ and $<T_m>$, as

$$\theta(r,z) = \frac{T(r,z) - <T_w>}{<T_w> - <T_m>}, \tag{22}$$

and the dimensionless local bulk mean temperature is defined as

$$\Theta_m(z) = \int_0^R \rho C_p u \theta dr \Big/ \int_0^R \rho C_p u dr. \tag{23}$$

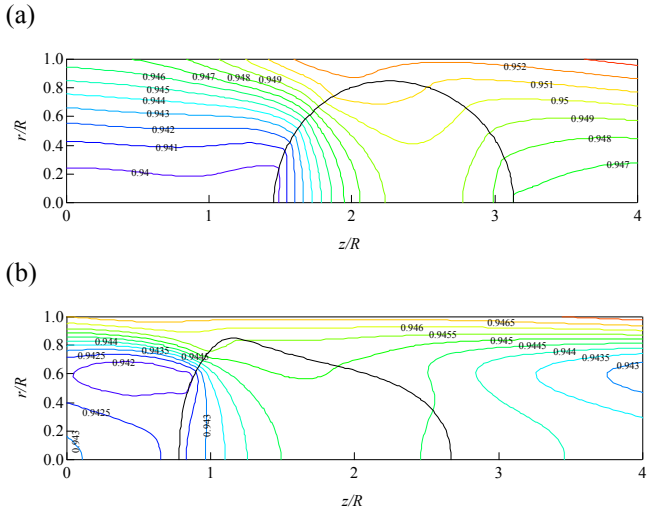

Fig. 7: Temperature contour at $\alpha = 0.2$ in $R = 10$ μm tube. (a) $-dP/dz = 85$ MPa/m; (b) 850 MPa/m. (The contour values are normalized by a certain reference temperature.)

In both cases shown in Fig. 8, the wall temperature locally peaks at the position where the tip of the bubble just passes. This observation qualitatively agrees with the experiment by Monde and Mitsutake [15], who measured the wall temperature fluctuations at different streamwise positions in mini channels. Beneath the bubble, the bulk mean temperature is close to the wall temperature as explained above. The overall temperature change is milder in the case with a higher pressure gradient (Fig. 8b). This is attributed to more active renewal of thermal layer due to the stronger circulation in the liquid slug.

The local Nusselt number defined as

$$Nu(z) = \frac{2Rh(z)}{\lambda} = \frac{2R\left.\frac{\partial \bar{\theta}}{\partial r}\right|_w}{\Theta_w(z) - \Theta_m(z)}, \tag{24}$$

is also shown in Fig. 8. Because the wall heat flux is constant and the pipe wall is always wet in the present simulation, the local Nusselt number is simply proportional to the inverse of difference between the local wall and bulk mean temperatures. In the region of liquid slug, Nu takes values close to that of the single phase flow, i.e., $Nu = 48/11$. The slightly higher value than that (especially in Fig. 8b) is due to mixing enhancement by the circulation. In the region where the bubble exists, Nu rises up to 20–30 due to the small difference between Θ_w and Θ_m. Accordingly, the domain-averaged Nusselt number, $<Nu>$, becomes also high as compared to single-phase flows; $<Nu> = 9.56$ and 10.67 for the cases of Figs. 8a and 8b, respectively.

The discussions made above are limited to flows in a periodic computational box, of which length is $L = 4R$. In two-phase flows, however, there may exist different flow patterns under a given set of conditions. In fact, recent experiment by Amador et al. [16] shows that different

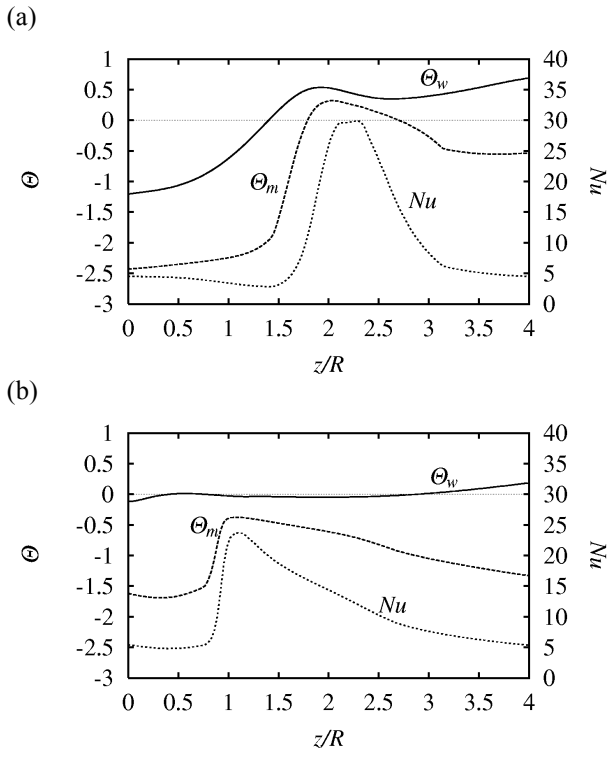

Fig. 8: Local wall and bulk-mean temperatures and local Nusselt number at $\alpha = 0.2$. (a) $-dP/dz = 85$ MPa/m; (b) 850 MPa/m.

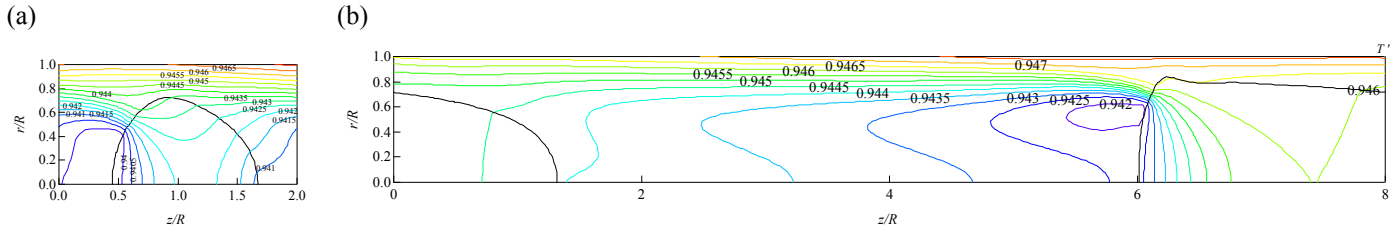

Fig. 9: Temperature contour at $\alpha = 0.2$ and $-dP/dz = 850$ MPa/m in $R = 10$ μm tube. (a) With computational domain of L/R=2; (b) L/R=8. (The contour values are normalized by a certain reference temperature.)

diameters of nozzle used for gas inlet result in different bubble periods under the same superficial velocities. Therefore, effects of the computational box size are briefly discussed here. Figure 9 shows the bubble shape and temperature contours computed under $\alpha = 0.2$ and $-dP/dz = 850$ MPa/m (the same condition as Fig. 7b), but with different lengths of computational box, $L = 2R$ and $L = 8R$. The resultant superficial velocities of gas and liquid are nearly unchanged. The bubble is elongated as the computational box size increases. The temperature contours have qualitative differences. The domain-averaged Nusselt number in the case of $L/R = 8$ is $\langle Nu \rangle = 10.23$, which is comparable to that with $L/R = 4$ reported above. For $L/R = 2$, however, $\langle Nu \rangle$ is 7.31. This indicates that the two-phase heat transfer is deteriorated when the period of bubbles becomes too short.

CONCLUSIONS

A series of numerical simulation are performed of air-water two-phase flows in a micro tube. The flow conditions are similar to those of the experiments by Serizawa et al. [8]. Unlike the experimental data, the global quantities computed in the present simulation are in good agreement with correlations proposed for macro-sized flow. It is argued that the difference of wall condition above the bubble, i.e., whether the wall is kept wet or dry, consistently explains this discrepancy. The local wall heat flux is very large beneath the bubble due to its small heat capacity and also enhanced in the liquid slug due to a circulating flow. The average Nusselt numbers are about 10 in the cases examined.

It is also found that the length of the computational domain, i.e., the period of bubbles, considerably affects the flow pattern and heat transfer characteristics. This suggests that one must carefully design both numerical and experimental conditions in order to quantitatively compare them. The solution to this problem is left as a future work.

ACKNOWLEDGMENT

This work was supported in part through the Grant-in-Aid for Young Researcher (B) by the Ministry of Education, Culture, Sports, Science and Technology of Japan (MEXT).

REFERENCES

1. N. Brauner and D. Moalem-Maron, Identification of the Range of Small Diameter Conduits, Regarding Two-Phase Flow Pattern Transition, *Int. Commun. Heat Mass Transfer*, vol. 19, pp. 29-39, 1992.
2. S. G. Kandlikar, Fundamental Issues Related to Flow Boiling in Minichannels and Microchannels, *Exp. Therm. Fluid Sci.*, vol. 26, 389-407, 2002.
3. M. Sussman, P. Smereka, and S. Osher, A Level Set Approach for Computing Solutions to Incompressible Two-Phase Flow, *J. Comput. Phys*., vol. 114, pp. 146-159, 1994.
4. J. U. Brackbill, D. B. Kothe, and C. A. Zemach, A Continuum Method for Modeling Surface Tension, *J. Comput. Phys.*, vol. 100, pp. 335-354, 1992.
5. A. A. Amsden and F. H. Harlow, The SMAC Method: A Numerical Technique for Calculating Incompressible Fluid Flows, Los Alamos Report, LA-4370, 1970.
6. T. Yabe, T. Aoki, G. Sakaguchi, P. Y. Wang, and T. Ishikawa, The Compact CIP (Cubic-Interpolated Pseudo-Particle) Method as a General Hyperbolic Solver, *Comput. Fluids*, vol. 19, pp. 421-431, 1991.
7. T. Himeno, T. Watanabe, and A. Konno, Numerical Analysis for Propellant Management in Liquid Rocket Tank, *AIAA Paper* 2001-3822, 2001.
8. A. Serizawa, Z. Feng, and Z. Kawara, Two-Phase Flow in A Microchannels, *Exp. Therm. Fluid Sci.*, vol. 26, pp. 703-714, 2002.
9. R. W. Lockhart and R. C. Martinelli, Proposed Correlation of Data for Isothermal Two-Phase Two-Component Flow in Pipes, *Chem. Eng. Prog.*, vol. 5, pp. 39-48, 1949.
10. D. Chisholm, A Theoretical Basis for the Lockhart-Martinelli Correlation for Two-Phase Flow, *Int. J. Heat Mass Transfer*, vol. 10, pp. 1767-1778, 1967.
11. K. Mishima and T. Hibiki, Some Characteristics of Air-Water Two-Phase Flow in Small Diameter Vertical Tubes, *Int. J. Multiphase Flow*, vol. 22, pp. 703-723, 1996.
12. T. C. Thulasidas, M. A. Abraham, and R. L. Cerro, Flow Patterns in Liquid Slugs During Bubble-Train Flow Inside Capillaries, *Chem. Eng. Sci.*, vol. 52, pp. 2947-2962, 1997.
13. S. Irandoust, and B. Andersson, Liquid Film in Taylor Flow Through A Capillary, *Ind. Eng. Chem. Res*., vol. 28, pp. 1684-1692, 1989.
14. A. A. Armand, G. G. Treschev, The Resistance During the Movement of A Two-Phase Systems in Horizontal Pipe, *Izv. Vses. Teplotek. Inst*., vol. 1, pp. 16-23, 1946.
15. M. Monde, and Y. Mitsutake, Enhancement of Heat Transfer due to Bubbles Passing Through a Narrow Vertical Rectangular Channel (Change in Heat Transfer along Flow) *Heat and Mass Transfer*, vol. 31, pp. 77-82, 1995.
16. C. Amador, W. Salman, S. Sanguanpiyapan, A. Gavriilidis, and P. Angeli, Effect of Gas/Liquid Inlet Conditions on the Mechanism of Taylor Flow Formation, *Proc. 5*th *Int. Conf. Multiphase Flow*, Paper 515, 2004.